

Entanglement robustness to excitonic spin precession in a quantum dot

Samir Bounouar,^{1,*} Gabriel Rein,¹ Kisa Barkemeyer,² Julian Schleibner,² Peter Schnauber,¹ Manuel Gschrey,¹ Jan-Hindrik Schulze,¹ André Strittmatter,¹ Sven Rodt,¹ Andreas Knorr,² Alexander Carmele,² and Stephan Reitzenstein¹

¹*Institut für Festkörperphysik, Technische Universität Berlin, 10623 Berlin, Germany*

²*Institut für Theoretische Physik, Technische Universität Berlin, 10623 Berlin, Germany*



(Received 3 February 2020; revised 17 April 2020; accepted 3 June 2020; published 13 July 2020)

A semiconductor quantum dot (QD) is an attractive resource to generate polarization-entangled photon pairs. We study the excitonic spin precession (flip-flop) in a family of QDs with different excitonic fine-structure splitting (FSS) and its impact on the entanglement of photons generated from the excitonic-biexcitonic radiative cascade. Our results reveal that coherent processes leave the time postselected entanglement of QDs with finite FSS unaffected while changing the eigenstates of the system. The flip-flop's precession is observed via quantum tomography through anomalous oscillations of the coincidences in the rectilinear basis. A theoretical model is constructed with the inclusion of an excitonic flip-flop rate and is compared with a two-photon quantum tomography measurement on a QD exhibiting the spin flip-flop mechanism. A generalization of the theoretical model allows estimating the degree of entanglement as a function of the FSS and the spin precession rate. For a finite temporal resolution, the negativity is found to be oscillating with respect to both the FSS and the spin precession rate. This oscillatory behavior disappears for perfect temporal resolution and maximal entanglement is retrieved despite the flip-flop process.

DOI: [10.1103/PhysRevB.102.045304](https://doi.org/10.1103/PhysRevB.102.045304)

I. INTRODUCTION

Quantum mechanical entanglement has proven to be a crucial prerequisite for experimental realizations of quantum communication protocols [1,2], quantum computing [3], or fundamental tests of quantum mechanics [4]. In this context, self-assembled semiconductor quantum dots (QDs) are excellent candidates for the on-demand generation of polarization-entangled photon pairs via the radiative exciton-biexciton cascade [5]. An excitonic fine-structure splitting (FSS) below the radiative linewidth has been considered as a prerequisite for the realization of such sources of entangled photon pairs [6–8]. More recently, time postselection of the excitonic wave packet has been applied as a which-path erasure for the generation of polarization-entangled photon pairs from QDs with significant FSS [9,10]. Since it requires no technologically demanding suppression of the FSS, the latter technique has proven to be very practical for the realization of complex quantum communication schemes [11] and is still unavoidable in the telecom wavelength range [12], even though these realizations were made possible at the cost of photon loss due to the postselection. Polarization entanglement is robust to pure dephasing when decoherence affects the excitonic (X) and the biexcitonic (XX) phase in the same manner [13–17]. This is the case for standard electron-phonon interactions in type III-V heterostructures and can be furthermore distilled via spectral filtering [18]. However, spin-flip-induced cross-dephasing processes still threaten the symmetry-imposed erasure of the which-path information and are believed to be the

main obstacle to the generation of entanglement with unity fidelity [19]. This is, in particular, true if the whole excitonic wave packet is collected in a time-integrated quantum state tomography setup [6–8,13,20]. If in contrast postselection is applied, the which-path information is again lost and maximum entanglement is established [9,10,21]. Conservation of entanglement even in the presence of spin precession has been overlooked until now since any hint of a spin flip inside a quantum dot usually discards it as a “bad candidate.” We show here that this preselection is not justified because spin precession is not harming the entanglement, provided a resolution precise enough is used in order to resolve the precession.

In this paper, we investigate the impact of the spin precession on postselected entanglement in a QD. We present a method for predicting the expected entanglement quality with the negativity as a measure for the degree of entanglement [22–24] as a function of the measured spin precession rates for a set of different QDs, considering a time postselection of the excitonic wave packet. In the derivation we make use of the Wigner-Weisskopf approximation assuming the dynamics to be Markovian. Beyond this limit, non-Markovianity could yield interesting effects such as the possibility to control the degree of entanglement via coherent time-delayed feedback [25–28]. Our method is tested on an InGaAs QD deterministically integrated into a microlens showing a non-null spin precession rate. It is then generalized by deriving the negativity as a function of the FSS and the spin precession rate analytically which is found to be oscillating for both parameters with a frequency defined by the actual experimental time resolution.

Interestingly, the precession of the excitonic spin configuration can be observed in the tomography measurements in the linear basis. In our case, the spin precession results in a unitary

*Corresponding author: Samir.bounouar@tu-berlin.de

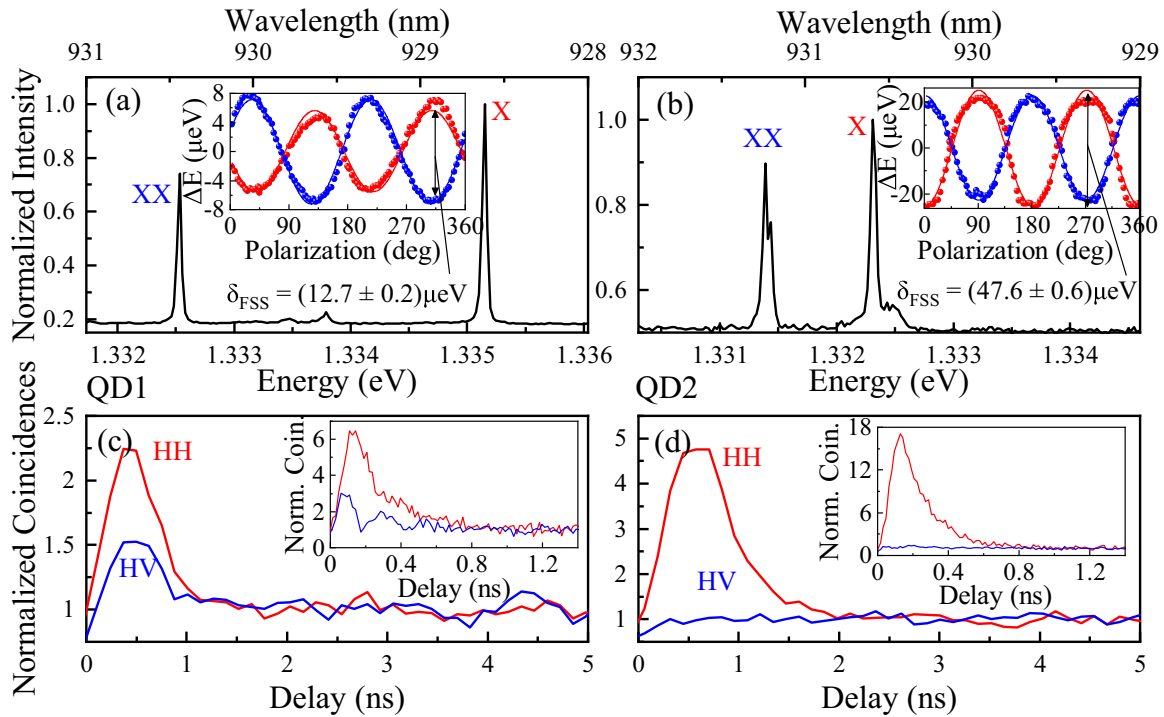


FIG. 1. Typical μ PL emission spectra of the studied quantum dots (a) QD1 with a FSS of $\delta_{\text{FSS}} = (12.7 \pm 0.2) \mu\text{eV}$ and (b) QD2 with a FSS of $\delta_{\text{FSS}} = (47.6 \pm 0.6) \mu\text{eV}$. Polarization-resolved measurements of the FSS are displayed in the inset of each graph. Polarization-resolved cross-correlation measurement of (c) QD1 and (d) QD2 in the HH basis (red) and in the HV basis (blue) obtained with SPCMs with 550 ps temporal resolution. The inset shows the same measurement using SNSPDs with a temporal resolution of 100 ps for comparison.

transformation, which is nondissipative and thus no obstacle to the time postselected generation of unity entanglement.

II. SAMPLE AND SETUP

Our experiments are carried out on self-assembled InGaAs/GaAs QDs grown by metal-organic chemical vapor deposition. The QDs are integrated deterministically into microlenses with a backside AlGaAs/GaAs distributed Bragg reflector by three-dimensional (3D) *in situ* electron-beam lithography [29]. The microlens sample is placed in a helium flow cryostat and operated at a temperature of 5 K. Microphotoluminescence (μ PL) measurements are performed with a standard cross-correlation spectroscopy setup, where detectors are silicon avalanche photodiode-based single-photon counting modules (SPCMs) with a temporal resolution of 550 ps [full width at half maximum (FWHM)]. A quantum tomography is realized via superconducting nanowire single-photon detectors (SNSPDs) with a temporal resolution of 100 ps (FWHM). The studied QDs are excited with a continuous-wave 780-nm laser diode.

III. SPIN PRECESSION RATE ESTIMATION

Figure 1 shows μ PL spectra of two different QDs, labeled QD1 [Fig. 1(a)] and QD2 [Fig. 1(b)], with a FSS of $\delta_{\text{FSS}} = (12.7 \pm 0.2) \mu\text{eV}$ and $\delta_{\text{FSS}} = (47.6 \pm 0.6) \mu\text{eV}$, respectively, as displayed in the insets. The spectra were obtained under nonresonant (780 nm) continuous-wave excitation. For both QDs, the two characteristic emission lines result from the

radiative recombination of the exciton (X) and the biexciton (XX) states. Excitonic spin precession rates can be estimated by measuring the XX and X photon correlations in the horizontal and the vertical basis where the basis states are set as aligned along the QD main axes. Figures 1(c) and 1(d) show the normalized coincidences measured between the XX and X photons with the XX photon triggering the correlation measurement. Photon bunching is not only found as expected in the horizontal-horizontal (HH) basis (in red) but also in the horizontal-vertical (HV) basis (in blue). This observation reveals the possibility for the excitonic population to transit from one excitonic component to the other, preventing the QD from emitting two copolarized photons which would be impossible without spin flips. The insets of Figs. 1(c) and 1(d) display the same polarization-resolved correlation measurement done with the superior resolution of the SNSPDs (100 ps) for QD1 and QD2, respectively. In the case of QD1, the spin precession related oscillations become visible for the HV correlations and a shoulder adds to the bunching observed for the HH correlations. These features are caused by a precession of the excitonic spins about the horizontal axis. In addition to the mixing of the excitonic components, a possible origin of the observed effect could be a Larmor-like precession about an effective magnetic field created by the surrounding nuclear spins [30]. The latter can be provided by the anisotropic nuclear spin distribution surrounding the QD [31]. It has been shown that the strength of the resulting effective magnetic field necessary for such a precession is reachable in QDs [32]. The exchange interaction between the electron and hole excitonic spins can also lead to their

relaxation through a mixing of the two excitonic components and could lead to the observed spin precession effect [33,34]. Such oscillations are not observed for QD2 in the inset of Fig. 1(d). The full tomography has been analyzed for QD2 in Ref. [10] and yielded in a near-unity entanglement after deconvolution of the experimental resolution, without any measurable effect of the decoherence on the entanglement fidelity. By comparing both bunchings, one can evaluate the excitonic spin precession rates. In the following, the spin precession rate will be studied by considering the ‘‘correlation value’’ g_{HV} defined as the ratio between the two bunchings observed for the cross correlations in the HH basis and in the HV basis after subtraction of the Poisson level: $g_{HV} = A_{HV}/A_{HH}$ with A_{HV} (A_{HH}) the time-integrated HV (HH) coincidences for positive delays [see Figs. 1(c) and 1(d)]. The correlation value g_{HV} is zero when no spin precession occur and reaches 1 when the spin precession rate is much larger than the excitonic decay rate. Figure 2 shows the different g_{HV} values evaluated for several QDs with different FSS. The two extreme situations in our family of QDs are represented by the two QDs marked as QD1 (highest correlation value) and QD2 (lowest correlation value). The geometry, or more precisely the anisotropy of the quantum dot shape, is the main factor determining the excitonic spin precession rate. In typical zinc-blende-based nanostructures any asymmetrical confinement leads to a mixing of the bright excitons [35]. This mixing is neither phonon assisted nor spin-orbit coupling based and does not involve the dark excitons. It stems most probably from the long-range part of the electron-hole exchange interaction [36]. The insets of Figs. 1(c) and 1(d) show the corresponding HH and HV correlation functions for these two QDs. The curves result from the theoretical model (described below) for different spin precession rates. They show that for a given spin precession rate the correlation value g_{HV} is decreasing with the FSS and allows an estimation of the occurring spin precession rate. The closest curve (represented

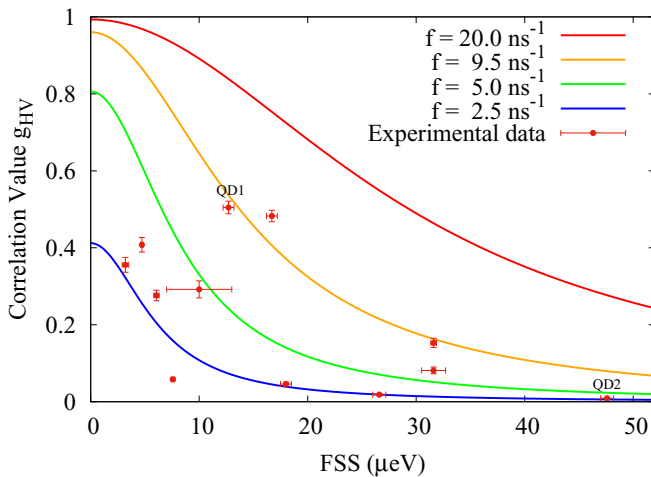


FIG. 2. Measured correlation values g_{HV} for several QDs as a function of their FSS. The two QDs discussed in the text are indicated as QD1 ($\delta_{\text{FSS}} = 12.7 \pm 0.2 \mu\text{eV}$) and QD2 ($\delta_{\text{FSS}} = 47.6 \pm 0.6 \mu\text{eV}$). The colored curves are extracted from the theoretical model for different spin precession rates.

in orange) to QD1 corresponds to a spin precession rate of $f = 9.5 \text{ ns}^{-1}$, which is consistent with the fit parameter used for the fitting of the quantum tomography.

IV. QUANTUM TOMOGRAPHY AND NEGATIVITY

To be able to understand the impact of the spin precession rate on the postselected entanglement, we develop a theoretical approach: We model the system in the Schrödinger picture and take into account a spin precession rate f and a FSS δ_{FSS} within a biexciton-cascade process. We show that the case with spin precession and FSS is equal to the case without spin precession but with FSS. Therefore, in the case of a time-resolved quantum state tomography setup, the spin precession rate has no detrimental effect if the temporal resolution is high in relation to the spin precession rate and FSS. The loss of which-path information is preserved under this particular unitary evolution and we can still find a high degree of entanglement. In order to show this, we map the biexciton-cascade process with a finite spin precession rate and FSS to the case of a diagonalized Hamiltonian in which the spin precession appears as a generalized FSS. This is done via the diagonalization of the Hamiltonian.

The Hamiltonian in the interaction picture reads

$$\begin{aligned}
 H/\hbar = & \frac{\delta_{\text{FSS}}}{2}(\sigma_{VV} - \sigma_{HH}) + f(\sigma_{VH} + \sigma_{HV}) \\
 & + g_0 \int d\omega (a_{\omega, BH}^\dagger \sigma_{HB} e^{i(\omega - \omega_{BX})t} \\
 & + a_{\omega, BV}^\dagger \sigma_{VB} e^{i(\omega - \omega_{BX})t} + \text{H.c.}) \\
 & + g_0 \int d\omega (a_{\omega, XH}^\dagger \sigma_{GH} e^{i(\omega - \omega_{XG})t} \\
 & + a_{\omega, XV}^\dagger \sigma_{GV} e^{i(\omega - \omega_{XG})t} + \text{H.c.}), \quad (1)
 \end{aligned}$$

where we spectrally distinguish the biexciton (B) from the exciton photons (X) with horizontal (H) or vertical (V) polarization in frequency mode ω which are annihilated (created) via $a_{\omega, B/XH/V}^\dagger$. The photon operators satisfy the bosonic commutation relation $[a_{\omega, im}, a_{\omega', jn}^\dagger] = \delta(\omega - \omega')\delta_{ij}\delta_{mn}$, $i, j \in \{B, X\}$, $m, n \in \{H, V\}$. Transitions between the electronic states are described by the flip operators $\sigma_{ij} = |i\rangle\langle j|$, $i, j \in \{B, X_H, X_V, G\}$ with $|B\rangle$ denoting the biexciton, $|X_H\rangle$ the horizontally polarized exciton, $|X_V\rangle$ the vertically polarized exciton, and $|G\rangle$ the ground state. For reasons of readability we replace the label of the excitonic states in the subscript by the respective direction of polarization $X_H \rightarrow H$, $X_V \rightarrow V$. The exciton energy $\hbar\omega_{XG}$ is centered between the energy of the horizontally polarized exciton state $\hbar\omega_{XG}^H = \hbar(\omega_{XG} - \delta_{\text{FSS}}/2)$ and the one of the vertically polarized exciton state $\hbar\omega_{XG}^V = \hbar(\omega_{XG} + \delta_{\text{FSS}}/2)$. The biexciton-exciton transition energy is $\hbar\omega_{BX} = \hbar(\omega_{XG} - \omega_{\text{bind}})$, where $\hbar\omega_{\text{bind}}$ describes the binding energy of the biexciton. The electron-photon interaction strength g_0 is related to the radiative decay constant Γ via $g_0 = \sqrt{\Gamma/\pi}$.

We first diagonalize the spin-flip part of the Hamiltonian via introducing other excitonic basis states

$$|X_{-}\rangle = \alpha|X_H\rangle - \beta|X_V\rangle, \quad (2)$$

$$|X_{+}\rangle = \beta|X_H\rangle + \alpha|X_V\rangle, \quad (3)$$

with $\alpha^2 = [1 + \delta_{\text{FSS}}/(2\Omega)]/2$, $\beta^2 = [1 - \delta_{\text{FSS}}/(2\Omega)]/2$, and the renormalized frequency $\Omega^2 = f^2 + (\delta_{\text{FSS}}/2)^2$. This transformation leads to a Hamiltonian which is diagonal in the spin-flip dynamics,

$$\begin{aligned} H/\hbar = & \Omega(\sigma_{++} - \sigma_{--}) \\ & + g_0 \int d\omega [\sigma_{-B}(\alpha a_{\omega,BH}^{\dagger} - \beta a_{\omega,BV}^{\dagger}) e^{i(\omega - \omega_{BX})t} \\ & + \sigma_{+B}(\beta a_{\omega,BH}^{\dagger} + \alpha a_{\omega,BV}^{\dagger}) e^{i(\omega - \omega_{BX})t} + \text{H.c.}] \\ & + g_0 \int d\omega [\sigma_{G-}(\alpha a_{\omega,XH}^{\dagger} - \beta a_{\omega,XV}^{\dagger}) e^{i(\omega - \omega_{XG})t} \\ & + \sigma_{G+}(\beta a_{\omega,XH}^{\dagger} + \alpha a_{\omega,XV}^{\dagger}) e^{i(\omega - \omega_{XG})t} + \text{H.c.}] \end{aligned} \quad (4)$$

We furthermore introduce other photonic operators,

$$a_{\omega,B/X+}^{\dagger} = \beta a_{\omega,B/XH}^{\dagger} + \alpha a_{\omega,B/XV}^{\dagger}, \quad (5)$$

$$a_{\omega,B/X-}^{\dagger} = \alpha a_{\omega,B/XH}^{\dagger} - \beta a_{\omega,B/XV}^{\dagger}. \quad (6)$$

Due to the definitions of α and β , these operators are bosonic operators and thus satisfy the commutation relation $[a_{\omega,im}^{\dagger}, a_{\omega',jn}^{\dagger}] = \delta(\omega - \omega')\delta_{ij}\delta_{mn}$, $i, j \in \{B, X\}$, $m, n \in \{+, -\}$. This can easily be shown by using $\alpha^2 + \beta^2 = 1$ and the commutation relations of the photon operators in the H/V basis.

Plugging in these photonic operators, the Hamiltonian reads

$$\begin{aligned} H/\hbar = & \Omega(\sigma_{++} - \sigma_{--}) \\ & + g_0 \int d\omega (\sigma_{-B} a_{\omega,B-}^{\dagger} e^{i(\omega - \omega_{BX})t} \\ & + \sigma_{+B} a_{\omega,B+}^{\dagger} e^{i(\omega - \omega_{BX})t} + \text{H.c.}) \\ & + g_0 \int d\omega (\sigma_{G-} a_{\omega,X-}^{\dagger} e^{i(\omega - \omega_{XG})t} \\ & + \sigma_{G+} a_{\omega,X+}^{\dagger} e^{i(\omega - \omega_{XG})t} + \text{H.c.}) \end{aligned} \quad (7)$$

Next, we calculate the combined state of the QD and the photonic reservoir. Assuming the system to initially be in the biexciton state, $|\Psi(0)\rangle = |B, \text{vac}\rangle$, the normalized wave function reads

$$\begin{aligned} |\Psi(t)\rangle = & e^{-2\Gamma t} |B, \text{vac}\rangle - i\sqrt{2\Gamma} e^{-\Gamma t} \int_0^t dt' e^{-\Gamma t'} \\ & \times [e^{-i\Omega(t-t')} |X_{+}, +(t')\rangle + e^{i\Omega(t-t')} |X_{-}, -(t')\rangle] \\ & - 2\Gamma \int_0^t dt' \int_0^{t'} dt'' e^{-\Gamma(t'+t'')} [e^{-i\Omega(t'-t'')} |+(t''), \\ & +(t')\rangle + e^{i\Omega(t'-t'')} |-(t''), -(t')\rangle]. \end{aligned} \quad (8)$$

Here, $|B, \text{vac}\rangle$ describes the system in the biexciton state and no photons in the reservoir, and $|X_{\pm}, \pm(t)\rangle$ refers to the system being in the \pm exciton state after the emission

of a \pm biexciton photon where we have defined the biexcitonic photon state as $|\pm(t)\rangle_B = (2\pi)^{-1/2} \int d\omega \exp[i(\omega - \omega_{BX})t] a_{\omega,\pm}^{\dagger} |\text{vac}\rangle$. The state $|\pm(t'), \pm(t)\rangle$ describes a \pm biexciton photon and a \pm exciton photon. The excitonic photon state is defined analogously as $|\pm(t)\rangle_X = (2\pi)^{-1/2} \int d\omega \exp[i(\omega - \omega_{XG})t] a_{\omega,\pm}^{\dagger} |\text{vac}\rangle$.

Looking at the above result we see that spin precessions do not change the physics of the biexciton cascade qualitatively as the solution is obtained by the same Hamiltonian to the case without spin precession but with finite FSS. In an integrated quantum state tomography, spin flips are detrimental to maximal entanglement just as an FSS is. For a time-resolved quantum state tomography, however, with a resolution high enough in relation to the spin precession rate and FSS, entanglement is preserved since which-path information is erased.

Using the state derived above, the time-resolved quantum state tomography can be calculated. In the following, we assume that the cascade process is finished. In this limit, the two-photon wave function reads in the basis of horizontally and vertically polarized photons

$$\begin{aligned} |\Psi(\infty)\rangle = & -2\Gamma \int_0^{\infty} dt' \int_0^{t'} dt'' e^{-\Gamma(t'+t'')} \\ & \times (\alpha^2 e^{i\Omega(t'-t'')} + \beta^2 e^{-i\Omega(t'-t'')}) |H(t''), H(t')\rangle \\ & - 2\Gamma \alpha \beta \int_0^{\infty} dt' \int_0^{t'} dt'' e^{-\Gamma(t'+t'')} \\ & \times (e^{-i\Omega(t'-t'')} - e^{i\Omega(t'-t'')}) |H(t''), V(t')\rangle \\ & - 2\Gamma \alpha \beta \int_0^{\infty} dt' \int_0^{t'} dt'' e^{-\Gamma(t'+t'')} \\ & \times (e^{-i\Omega(t'-t'')} - e^{i\Omega(t'-t'')}) |V(t''), H(t')\rangle \\ & - 2\Gamma \int_0^{\infty} dt' \int_0^{t'} dt'' e^{-\Gamma(t'+t'')} \\ & \times (\alpha^2 e^{-i\Omega(t'-t'')} + \beta^2 e^{i\Omega(t'-t'')}) |V(t''), V(t')\rangle. \end{aligned} \quad (9)$$

We can rewrite the wave function as

$$\begin{aligned} |\Psi(\infty)\rangle = & \int_0^{\infty} dt' \int_0^{t'} dt'' [P_D(t'', t') |H(t''), H(t')\rangle \\ & + P_D^*(t'', t') |V(t''), V(t')\rangle] \\ & + \int_0^{\infty} dt' \int_0^{t'} dt'' [P_{ND}(t'', t') |H(t''), V(t')\rangle \\ & - P_{ND}^*(t'', t') |V(t''), H(t')\rangle], \end{aligned} \quad (10)$$

with

$$\begin{aligned} P_D(t'', t') = & -2\Gamma e^{-\Gamma(t'+t'')} \\ & \times \left\{ \cos[\Omega(t' - t'')] + i \frac{\delta_{\text{FSS}}}{2\Omega} \sin[\Omega(t' - t'')] \right\}, \end{aligned} \quad (11)$$

$$P_{ND}(t'', t') = i2\Gamma \frac{f}{\Omega} e^{-\Gamma(t'+t'')} \sin[\Omega(t' - t'')]. \quad (12)$$

The detection of a biexciton (B) or exciton (X) photon with polarization H/V at time t_D can be described via the operators

$$D_{B\ H/V}^{(+)}(t_D) = \frac{1}{\sqrt{2\pi}} \int d\omega e^{-i(\omega - \omega_{BX})t_D} a_{\omega, B\ H/V}, \quad (13)$$

$$D_{X\ H/V}^{(+)}(t_D) = \frac{1}{\sqrt{2\pi}} \int d\omega e^{-i(\omega - \omega_{XG})t_D} a_{\omega, X\ H/V}. \quad (14)$$

Using the relation

$$D_{XH}^{(+)}(t_X) D_{BH}^{(+)}(t_B) |H(t'')H(t')\rangle = \delta(t_X - t'')\delta(t_B - t') |\text{vac}\rangle \quad (15)$$

and analogous relations for the other polarization directions, we can describe the detection of the exciton photon at t_X and the detection of the biexciton photon at t_B in the basis $\{|HH\rangle, |HV\rangle, |VH\rangle, |VV\rangle\}$ as

$$|\Psi(t_X, t_B)\rangle = [P_D(t_X, t_B), P_{ND}(t_X, t_B), -P_{ND}^*(t_X, t_B), P_D^*(t_X, t_B)]^T. \quad (16)$$

The corresponding measurement matrix can be constructed via

$$P_{im, jn}(t_X, t_B) = \langle i\ m|\Psi(t_X, t_B)\rangle \langle \Psi(t_X, t_B)|j\ n\rangle, \quad (17)$$

with $i, j, n \in \{H, V\}$. Note that if we normalize the above state and matrix, the conditional probability to measure the photon pair in certain directions of polarization given that we measure them at time t_X and t_B can be calculated from their elements. Convoluting the elements of the measurement matrix with the system response function we can fit the experimentally determined tomography. Figure 3(a) shows the 16

polarization cross-correlation measurements of QD1 necessary for the full tomography [37]. The black lines represent the experimental data, and the red lines are obtained from the analytical model using the experimental parameters $\Gamma = 2.4\ \text{ns}^{-1}$ and $\delta_{\text{FSS}} = 12.7\ \mu\text{eV}$ with an estimate of $f = 9.5\ \text{ns}^{-1}$ for the spin precession rate. Note that pure dephasing processes are not considered as they do not affect the entanglement [13–17], while correlations in the R/L and D/A basis are accounting for the quantum correlations. Oscillations in these bases are evidence of excitonic phase precession due to the presence of finite FSS. Correlations in the H/V basis are classical, and these oscillations are due to the presence of spin-flip precession. Since the two processes are being evidenced in two different bases, we can study them separately. Overall, we obtain a very good agreement between experiment and theory. However, for some elements of the two-photon density matrix (e.g., RV and VR), the bunching values measured in the HV and VH correlations are underestimated by the fits. This discrepancy could be explained by some unintentional fluctuations of the excitation power which is influencing the bunching amplitude of the correlations in these bases. A wrong preparation of the R basis during the measurement could be another experimental source of error. The biexciton preparation in the model is made in a deterministic way which is different from the experimental conditions, where the nonresonant continuous excitation of the biexciton is probabilistic. These quantitative discrepancies mainly in the RV and VR element do not change the qualitative result of our study, which remains very general that coherent spin-flip precession is not detrimental to the degree of polarization entanglement. However, the discrepancies prove that a more detailed theoretical model is necessary to take into account incoherent processes which are responsible for the initial bunching, e.g., in the RV and VR elements.

Figure 3(b) shows the numerically obtained negativity \mathcal{N} as a function of the delay. The negativity is a measure of the degree of entanglement of the two photons. It is defined as the absolute value of the negative eigenvalue of the partially transposed two-photon density matrix [24]. A value of $\mathcal{N} > 0$ signifies an entangled two-photon state with maximal entanglement at $\mathcal{N} = 1/2$. If perfect time resolution is assumed, the negativity is maximal (i.e., $\mathcal{N} = 1/2$), independent of the delay since the two-photon wave function remains maximally entangled [cf. Eq. (8)]. Spin precession processes and FSS do not change the symmetry of the problem if no time average is applied. As a result, the negativity, as a basis-independent measure for the degree of polarization entanglement, is not changed whether the system is expressed in the $\{H, V\}$ or in the $\{+, -\}$ basis. However, for finite time resolution the spin precession and the FSS dynamics result in a reduced negativity. If the photon-detection events are not postselected but integrated and therefore averaged, spin precession dynamics have a detrimental influence. In the case of temporal post-selection for nonzero FSS, oscillations corresponding to the precession of the excitonic phase are observed in the circular (RR) and in the diagonal basis (DD), as is also the case in the absence of spin precession. Moreover, due to the spin precession process, oscillations can also be observed in the rectilinear basis (VH, HV, VV , and HH). Such oscillations are a direct consequence of the excitonic spin precessions and

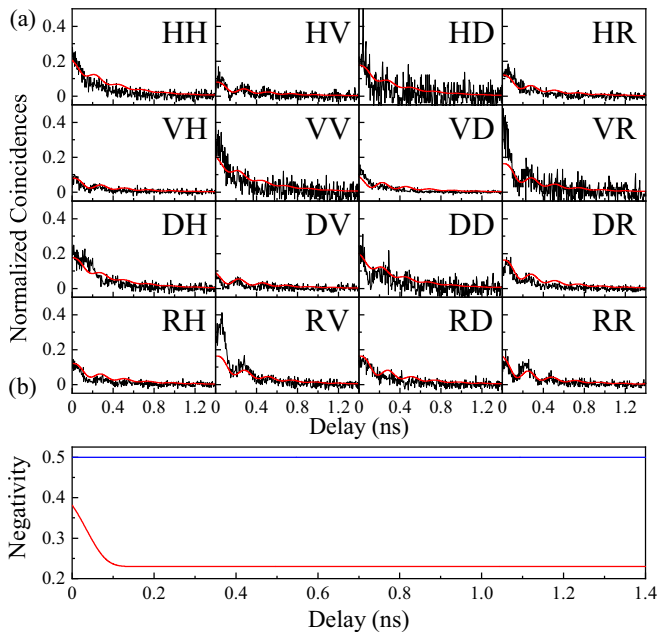


FIG. 3. (a) Sixteen polarization-resolved measurements representing the full tomography of QD1. The red curves result from the fitting model taking the spin precession processes in the QD into account and convoluted to the setup resolution. This fitting is used to calibrate the model and to extrapolate it for the other QDs studied here. (b) Extrapolated negativity as a function of the delay for a perfect temporal resolution (blue) and a 100 ps resolution (red).

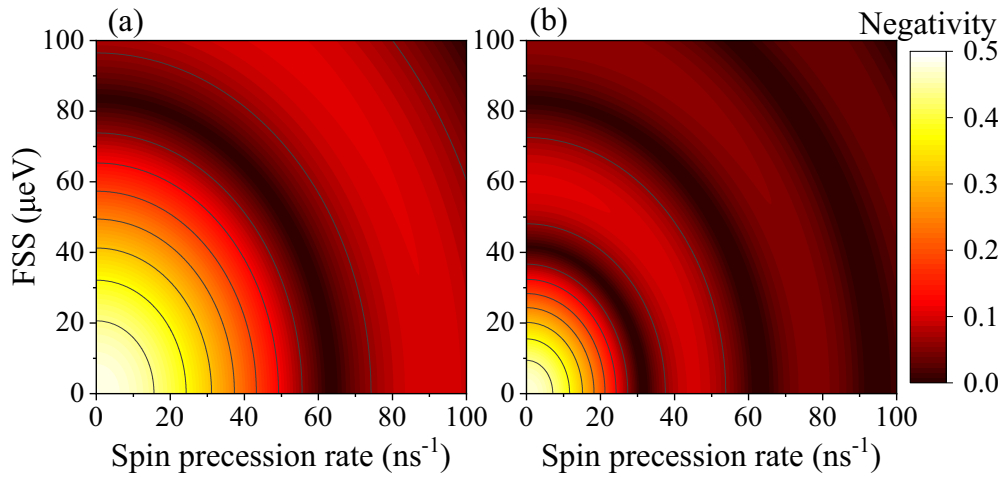


FIG. 4. Negativity as a function of the spin precession rate and the FSS for a resolution of (a) 50 ps and of (b) 100 ps.

are not observed in the case of spin precession rate zero. From these data and the theory, one can at the same time test and calibrate the model and evaluate the quality of the emitted entanglement by this QD (QD1) in terms of the negativity [22–24]. In the following, we extrapolate the model to the general evaluation of the entanglement as a function of the FSS and the spin precession rate for any QD.

To evaluate the degree of entanglement of the two photons theoretically, we look at the normalized density matrix $\rho_N = \rho/\text{tr}(\rho)$ and calculate its negativity. If we assume a perfect resolution of the detection process, we obtain a negativity of

$$\mathcal{N}[\rho_N(t_X, t_B)] = \frac{1}{2} \quad (18)$$

for all times t_X, t_B . Hence, we see that maximal entanglement is preserved despite the spin precession. If we take into account that in realistic experiments we can only determine the time difference between the detection events with a resolution of ΔT , we have to evaluate the negativity of the averaged density matrix,

$$\rho_{AV}(t, \Delta T) = \frac{1}{\Delta T} \int_t^{t+\Delta T} dt \rho_N(t, 0), \quad (19)$$

where we set the time of detection of the biexciton photon to zero. The evaluation of the negativity yields

$$\mathcal{N}[\rho_{AV}(t, \Delta T)] = \frac{1}{2} |\text{sinc}(\Omega \Delta T)|. \quad (20)$$

Figure 4 shows the negativity as a function of the spin precession rate and the FSS for a given temporal resolution. This graph gives an overview of the negativity which can be expected depending on the FSS and spin precession rates characteristic for QDs for two different resolutions [Fig. 4(a) for a 50 ps resolution and Fig. 4(b) for a 100 ps resolution]. The overall entanglement quality is degraded as the FSS and the spin precession rate are increased. This degradation is modulated by oscillations with respect to the FSS and the spin precession rate. As can be deduced from the equation above, the temporal resolution of the detectors defines the frequency of these oscillations.

Perfect temporal resolution, that is, $\Delta T = 0$, leads to a negativity being equal to $1/2$, which means that perfect

entanglement can be measured, provided that no additional dephasing processes need to be taken into account.

Therefore, in the case of a perfect time postselection, this mechanism is not detrimental for the generation of entanglement from QDs.

V. CONCLUSION

We investigated the entanglement in QDs showing spin precession processes. The precession of the excitonic spins has been experimentally evidenced through the observation of anomalous oscillations in the rectilinear basis correlations. The associated quantum tomography measurement allows for studying the impact of spin precession processes on the entanglement. Noncoherent spin flips, phonon mediated, for example, such as single-electron spin flip towards the dark exciton, can break the quantum dot symmetry and can be detrimental to entanglement [13]. However, such processes are slow compared to the excitonic lifetime and our study shows that they do not occur during the radiative cascade's recombination. In fact, no additional decoherence is needed in the model in order to explain the data. This observation is confirmed by another work investigating the effect of spin dynamics on entanglement (no spin precession is observed here, though) [38]. We determined and studied the entanglement quality which can be ideally expected from a QD suffering from spin precession for a given temporal resolution. The theoretical model shows that the spin precession rate acts the same way as a nonzero FSS and that a perfect temporal resolution would allow for ideal entanglement independent of the spin precession rate. Temporal postselection is therefore effective at providing perfect entanglement even in the presence of coherent processes modifying the eigenstates of the system since the latter are a coherent superposition of the excitonic states. Noncoherent processes affecting the excitonic and biexcitonic phases differently are the last remaining phenomena which cannot be effectively suppressed by postselection. A coherent population of the biexciton and its coherent control through two-photon excitation or pulse-echo techniques [39] are in this case relevant to complement it.

ACKNOWLEDGMENTS

The research leading to these results has received funding from the European Research Council (ERC) under the European Union's Seventh Framework ERC Grant Agreement No. 615613 and from the German Research Foundation via

Project No. RE2974/12-1. We also acknowledge support from the Deutsche Forschungsgemeinschaft (DFG) through the Collaborative Research Center CRC787. A.C. acknowledges support from the Deutsche Forschungsgemeinschaft (DFG) through the Collaborative Research Center CRC910.

-
- [1] E. Knill, R. Laflamme, and G. J. Milburn, *Nature (London)* **409**, 46 (2001).
- [2] H. J. Kimble, *Nature (London)* **453**, 1023 (2008).
- [3] J.-W. Pan, Z.-B. Chen, C.-Y. Lu, H. Weinfurter, A. Zeilinger, and M. Żukowski, *Rev. Mod. Phys.* **84**, 777 (2012).
- [4] W. Tittel and G. Weihs, *Quantum Inf. Comput.* **1**, 3 (2001).
- [5] O. Benson, C. Santori, M. Pelton, and Y. Yamamoto, *Phys. Rev. Lett.* **84**, 2513 (2000).
- [6] N. Akopian, N. H. Lindner, E. Poem, Y. Berlatzky, J. Avron, D. Gershoni, B. D. Gerardot, and P. M. Petroff, *Phys. Rev. Lett.* **96**, 130501 (2006).
- [7] R. J. Young, R. M. Stevenson, P. Atkinson, K. Cooper, D. A. Ritchie, and A. J. Shields, *New J. Phys.* **8**, 29 (2006).
- [8] M. Müller, S. Bounouar, K. D. Jöns, M. Glässl, and P. Michler, *Nat. Photonics* **8**, 224 (2014).
- [9] R. Winik, D. Cogan, Y. Don, I. Schwartz, L. Gantz, E. R. Schmidgall, N. Livneh, R. Rapaport, E. Buks, and D. Gershoni, *Phys. Rev. B* **95**, 235435 (2017).
- [10] S. Bounouar, C. de la Haye, M. Strauß, P. Schnauber, A. Thoma, M. Gschrey, J.-H. Schulze, A. Strittmatter, S. Rodt, and S. Reitzenstein, *Appl. Phys. Lett.* **112**, 153107 (2018).
- [11] M. Zopf, R. Keil, Y. Chen, J. Yang, D. Chen, F. Ding, and O. G. Schmidt, *Phys. Rev. Lett.* **123**, 160502 (2019).
- [12] J. Huwer, R. M. Stevenson, J. Skiba-Szymanska, M. B. Ward, A. J. Shields, M. Felle, I. Farrer, D. A. Ritchie, and R. V. Pentyl, *Phys. Rev. Appl.* **8**, 024007 (2017).
- [13] R. M. Stevenson, A. J. Hudson, A. J. Bennett, R. J. Young, C. A. Nicoll, D. A. Ritchie, and A. J. Shields, *Phys. Rev. Lett.* **101**, 170501 (2008).
- [14] A. Carmele and A. Knorr, *Phys. Rev. B* **84**, 075328 (2011).
- [15] D. Reiter, T. Kuhn, and V. M. Axt, *Adv. Phys.: X* **4**, 1655478 (2019).
- [16] T. Seidelmann, F. Ungar, M. Cygorek, A. Vagov, A. M. Barth, T. Kuhn, and V. M. Axt, *Phys. Rev. B* **99**, 245301 (2019).
- [17] U. Hohenester, G. Pfanner, and M. Seliger, *Phys. Rev. Lett.* **99**, 047402 (2007).
- [18] E. del Valle, *New J. Phys.* **15**, 025019 (2013).
- [19] D. Huber, M. Reindl, S. F. Covre da Silva, C. Schimpf, J. Martín-Sánchez, H. Huang, G. Piredda, J. Edlinger, A. Rastelli, and R. Trotta, *Phys. Rev. Lett.* **121**, 033902 (2018).
- [20] A. Carmele, F. Milde, M.-R. Dachner, M. B. Harouni, R. Roknizadeh, M. Richter, and A. Knorr, *Phys. Rev. B* **81**, 195319 (2010).
- [21] M. A. Versteegh, M. E. Reimer, K. D. Jöns, D. Dalacu, P. J. Poole, A. Gulinatti, A. Giudice, and V. Zwiller, *Nat. Commun.* **5**, 5298 (2014).
- [22] F. Verstraete, K. Audenaert, J. Dehaene, and B. De Moor, *J. Phys. A: Math. Gen.* **34**, 10327 (2001).
- [23] S. Lee, D. P. Chi, S. D. Oh, and J. Kim, *Phys. Rev. A* **68**, 062304 (2003).
- [24] A. Peres, *Phys. Rev. Lett.* **77**, 1413 (1996).
- [25] K. Barkemeyer, R. Finsterhölzl, A. Knorr, and A. Carmele, *Adv. Quantum Technol.* **3**, 1900078 (2019).
- [26] A. Carmele and S. Reitzenstein, *Nanophotonics* **8**, 655 (2019).
- [27] M. Strauß, A. Carmele, J. Schleichner, M. Hohn, C. Schneider, S. Höfling, J. Wolters, and S. Reitzenstein, *Phys. Rev. Lett.* **122**, 107401 (2019).
- [28] S. M. Hein, F. Schulze, A. Carmele, and A. Knorr, *Phys. Rev. Lett.* **113**, 027401 (2014).
- [29] M. Gschrey, A. Thoma, P. Schnauber, M. Seifried, R. Schmidt, B. Wohlfeil, L. Krüger, J.-H. Schulze, T. Heindel, S. Burger *et al.*, *Nat. Commun.* **6**, 7662 (2015).
- [30] A. W. Overhauser, *Phys. Rev.* **92**, 411 (1953).
- [31] C. Hinz, P. Gumbsheimer, C. Traum, M. Holtkemper, B. Bauer, J. Haase, S. Mahapatra, A. Frey, K. Brunner, D. E. Reiter *et al.*, *Phys. Rev. B* **97**, 045302 (2018).
- [32] A. I. P. Maletinsky, in *Single Semiconductor Quantum Dots*, edited by P. Michler (Springer, Berlin, 2009), Chap. 5, pp. 145–184.
- [33] M. Z. Maialle, E. A. de Andrada e Silva, and L. J. Sham, *Phys. Rev. B* **47**, 15776 (1993).
- [34] H. Nickolaus, H.-J. Wünsche, and F. Henneberger, *Phys. Rev. Lett.* **81**, 2586 (1998).
- [35] E. L. Ivchenko, *Phys. Status Solidi A* **164**, 487 (1997).
- [36] T. Takagahara, *Phys. Rev. B* **62**, 16840 (2000).
- [37] D. F. V. James, P. G. Kwiat, W. J. Munro, and A. G. White, *Phys. Rev. A* **64**, 052312 (2001).
- [38] A. Fognini, A. Ahmadi, M. Zeeshan, J. T. Fokkens, S. J. Gibson, N. Sherlekar, S. J. Daley, D. Dalacu, P. J. Poole, K. D. Jöns, V. Zwiller, and M. E. Reimer, *ACS Photonics* **6**, 1656 (2019).
- [39] H. Jayakumar, A. Predojević, T. Huber, T. Kauten, G. S. Solomon, and G. Weihs, *Phys. Rev. Lett.* **110**, 135505 (2013).